Available online at www.sciencedirect.com
ScienceDirect
International Journal of Thermal Sciences 46 (2007) 48–56
International Journal of Thermal Sciences
www.elsevier.com/locate/ijts

Mathematical modeling of transport phenomena in porous SOFC anodes

M.M. Hussain [a], X. Li [a], I. Dincer [b,*]

[a] *Department of Mechanical Engineering, University of Waterloo, Waterloo, Ontario N2L 3G1, Canada*
[b] *Faculty of Engineering and Applied Science, University of Ontario Institute of Technology (UOIT) Oshawa, Ontario L1H 7K4, Canada*

Received 28 November 2005; accepted 12 April 2006

Available online 5 June 2006

Abstract

In the present study, a mathematical model describing the transport of multi-component species inside porous SOFC anodes is developed. The model considers the reaction zone layer as a distinct volume rather than a mere mathematical surface (boundary condition) as treated in the existing models. The reaction zone layer is a relatively thin layer in the vicinity of electrolyte where electrochemical H_2 oxidation takes place to produce electrons and water vapor. The model also incorporates the effect of Knudsen diffusion in the porous electrode and reaction zone layers. Simulations are performed using multi-component ethanol reformate fuel to predict the distribution of multi-component species in the electrode and reaction zone layers at different loads (current densities). In addition, the effect of shift reaction on the concentration overpotential is examined. Moreover, the effect of treating reaction zone layer as a discrete volume is investigated.

Keywords: Modeling; Multi-component species; Reaction zone layer; SOFC anode

1. Introduction

Solid oxide fuel cell (SOFC) is a solid-state ceramic cell, operating at the high temperature of around 1000 °C. Both hydrogen and carbon monoxide can be used as a fuel, either directly or indirectly through the water-gas shift reaction, thus providing the flexibility on fuel. SOFC is promising for electric utility power generation in both large central power plants and decentralized generation units [1].

Because of simplicity in manufacturing and higher power density, planar-type design of SOFC has received much attention recently [2,3]. However, the commercialization of planar-type SOFC has some technical challenges due to high temperature operation such as internal stresses in cell components arising from thermal shocks or heat cycles, mismatch in thermal expansion coefficient among cell components and non-homogeneous temperature distribution inside the cell. In order to overcome the problems associated with high temperature operation of SOFC and enhance its performance, presently much of the research is focused on developing new materials and configurations which provides better or similar performance at reduced operating temperatures [4,5]. The other consequence of reducing the operating temperature is the reduction in the ionic conductivity of the electrolyte resulting in higher ohmic overpotential, which can be minimized by using electrode supported (anode or cathode) configuration of SOFC, wherein thin electrolyte of thicknesses around 20 μm are deposited on the thick anode or cathode and thereby reduces the ohmic overpotential at reduced temperatures. However, in electrode-supported cells (anode or cathode), it is reported that concentration overpotential due to resistance to transport of reactants to the reaction sites becomes significant [5,6]. Therefore, the thicknesses of different components of SOFC should be optimized to minimize both ohmic and concentration overpotentials and provides better performance.

The resistance to the flow of reactant species through the void spaces of the porous layers results in lower reactant concentration at the reaction sites. The loss in cell potential due to mass transfer limitation is referred to as concentration overpotential. The accurate determination of the rate of mass transport inside the porous electrodes is extremely important to minimize the concentration overpotential at higher current densities. The

* Corresponding author.
E-mail addresses: mmhussain@uwaterloo.ca (M.M. Hussain), x6li@uwaterloo.ca (X. Li), ibrahim.dincer@uoit.ca (I. Dincer).

1290-0729/$ – see front matter
doi:10.1016/j.ijthermalsci.2006.04.004

Nomenclature

A_v	reactive surface area per unit volume	$m^2\,m^{-3}$	
c_{H_2}	hydrogen concentration	$mole\,m^{-3}$	
$c_{H_2,ref}$	reference hydrogen concentration	$mole\,m^{-3}$	
d_p	diameter of the pore	μm	
D_{ij}	ordinary diffusion coefficient	$m^2\,s^{-1}$	
$D_{Kn,i}$	Knudsen diffusion coefficient	$m^2\,s^{-1}$	
$\wp_{ij}$	effective diffusion coefficient	$m^2\,s^{-1}$	
F	Faraday's constant, 96 487 C mole^{-1}		
J	current density	$A\,m^{-2}$	
$\mathcal{J}_a$	volumetric current density in the anode	$A\,m^{-3}$	
J_e	electronic current density	$A\,m^{-2}$	
J_i	ionic current density	$A\,m^{-2}$	
$J_{0,ref}^{H_2}$	reference exchange current density	$A\,m^{-2}$	
k_{bs}	backward reaction rate constant	$J\,mole^{-1}$	
k_{fs}	forward reaction rate constant	$J\,mole^{-1}$	
K_{ps}	equilibrium constant for shift reaction		
l_e	volume fraction of the electrolyte		
M_i	molecular weight of species i	$kg\,mole^{-1}$	
n	moles of electrons transferred per mole reactant		
N_i	diffusive flux of species i,	$mole\,m^{-2}\,s^{-1}$	
R	universal gas constant, 8.3143 J mole^{-1} K^{-1}		
$\Re_a$	volumetric current density produced in the anode	$A\,m^{-3}$	
r_s	volumetric shift reaction rate	$kg\,m^{-3}\,s^{-1}$	
$\dot{S}_{s,i}$	species source term	$kg\,m^{-3}\,s^{-1}$	
T	temperature	K	
V_i	diffusive velocity of species i	$m\,s^{-1}$	
x	rectangular coordinate	m	
x_i	mole fraction of species i		

Greek symbols

α	charge transfer coefficient	
ε	porosity	
ϕ_e	electronic potential	V
ϕ_i	ionic potential	V
Φ	volume fraction of electron conducting particles in reaction zone layer	
γ_{H_2}	reaction order	
κ	ionic conductivity	$S\,m^{-1}$
η_{con}	concentration overpotential	V
ρ_i	partial density of species i	$kg\,m^{-3}$
σ	electronic conductivity	$S\,m^{-1}$
τ	tortuosity	

Subscripts

bl	electrode (backing) layer
rl	reaction zone layer

Superscripts

eff	effective

rate of mass transport inside the porous electrodes of SOFC depends on the operating and design parameters such as temperature, pressure, fuel composition, pore size, porosity and tortuosity [6].

Recently, transport of gaseous species inside the porous anode has been studied by various researchers [6–8]. Yakabe et al. [6] and Lehnert et al. [7] used mass transport models similar to dusty–gas model, whereas Suwanwarangkul et al. [8] used three different models such as Fick's model, dusty–gas model and Stefan–Maxwell model to simulate two binary systems (H_2–H_2O and CO–CO_2) and a ternary system (H_2–H_2O–Ar). Yakabe et al. [6] and Lehnert et al. [7] included water-gas shift reaction in their model but Suwanwarangkul et al. [8] did not consider it. The similarity in their models is the consideration of reaction zone as a mathematical surface, treating it as a boundary condition. However, for composite electrodes such as those in SOFCs, the reaction zone is spread out into the electrode some distance from the electrolyte/electrode interface [7,9–11].

The objective of this study is to develop a mathematical model describing the transport of multi-component species inside porous SOFC anodes, which includes reaction zone layer as a discrete volume rather than a mathematical surface as treated in the existing models. The model is fuel flexible, which means not only pure H_2 but also any reformate, which is composed of H_2, H_2O, CO and CO_2 can be used as a fuel. Therefore, in the present study, the composition of ethanol reformate fuel is used to predict the distribution of multi-component species in the electrode and reaction zone layers at different current densities. Moreover, it is aimed to examine the effect of shift reaction and finite reaction zone layer on the concentration overpotential.

2. Modeling

The different layers on the anode side of an anode-supported SOFC are illustrated in Fig. 1. The present model deals with porous anode only, which is classified as anode electrode layer and anode reaction zone layer. The additional layer shown between the electrode and electrolyte is a region where the electrochemical oxidation takes place to produce electrons and water vapor. Consideration of reaction zone layer as a finite volume adds complexities to the mathematical model since conservation equations have to be solved along with chemical and electrochemical reactions.

The assumptions considered in the mathematical formulation are steady state cell operation and one-dimensional variation of parameters in x-direction only as shown in Fig. 1. The temperature and total pressure are assumed to be uniform throughout the anode. The momentum of gaseous species in porous anode is assumed to be negligible, implying the transport of reactant species to the reaction sites in the reaction zone layer is predominantly by diffusion. The reactant gas mixtures are approximated as ideal gases with negligible viscous, Soret, Dofour, and gravity effects. The anode reaction zone

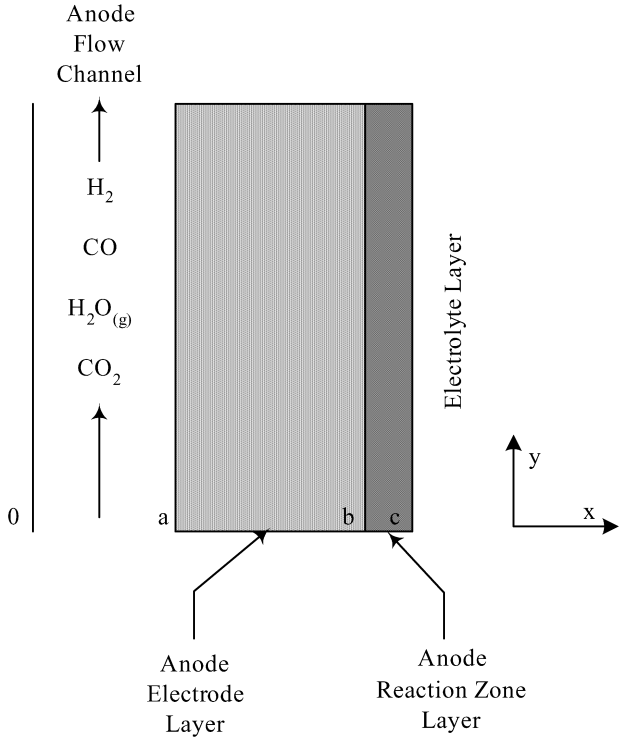

Fig. 1. Anode side of solid oxide fuel cells.

layer consists of a mixture of electron-conducting particles, ion-conducting particles and void space occupied by gaseous species. Moreover, it is assumed that there is no electrochemical oxidation of CO in the anode reaction zone.

By applying the conservation of species equation together with the modified Stefan–Maxwell equations incorporating Knudsen diffusion for multi-component gas diffusion, the general Butler–Volmer equation for the electrochemical reaction in the reaction zone layer and electroneutrality, the mathematical model for the processes occurring in the anode electrode and reaction zone layers is formulated. The governing equations are then described as follows:

Species:

$$\nabla \cdot (\rho_i V_i) = \dot{S}_{s,i} \tag{1}$$

Electronic charge – electrode layer:

$$\nabla \cdot J_e = 0 \tag{2}$$

Electronic charge – reaction zone layer:

$$\nabla \cdot J_e = \Re_a \tag{3}$$

Ionic charge – reaction zone layer:

$$\nabla \cdot J_i = -\Re_a \tag{4}$$

where ρ_i is the partial density of species i, V_i is the species diffusion velocity, $\dot{S}_{s,i}$ is the species source term representing the rate of production or consumption of species due to water–gas shift reaction in the electrode layer and production or consumption of species due to water–gas shift reaction and H_2 oxidation reaction in the reaction zone layer, J_e is the electronic current density, J_i is the ionic current density and $\Re_a$ is the volumetric current density produced in the reaction zone layer due to H_2 oxidation, which is given by the general Butler–Volmer equation expressed as

$$\Re_a = A_v J_{0,ref}^{H_2} \left(\frac{c_{H_2}}{c_{H_2,ref}}\right)^{\gamma_{H_2}} \left\{ \exp\left(\frac{\alpha n F(\phi_i - \phi_e)}{RT}\right) - \exp\left(-\frac{(1-\alpha) n F(\phi_i - \phi_e)}{RT}\right)\right\} \tag{5}$$

where A_v is the reactive surface area per unit volume, $J_{0,ref}^{H_2}$ is the reference exchange current density at the reference concentration $c_{H_2,ref}$, α is the charge transfer coefficient, n is the moles of electron produced per mole of reactant consumed, F is the Faraday's constant (96 487 C mole^{-1}), ϕ_e and ϕ_i are electronic and ionic potentials, respectively.

The diffusion flux can be determined using the Stefan–Maxwell equations for multi-component systems involving n species, expressed as [12]:

$$-c\nabla x_i = \sum_{j=1, i\neq j}^{n} \frac{1}{D_{ij}} (x_j \vec{N}_i - x_i \vec{N}_j) \tag{6}$$

where c is the concentration of the mixture, D_{ij} is the ordinary or binary diffusion coefficient of species i in j, x_i is the mole fraction of species i, and $\vec{N}_i$ is the diffusion flux of species i.

Typically, in SOFC electrodes both ordinary and Knudsen diffusion occurs simultaneously [13]. In order to account Knudsen diffusion effect, the above model is modified and expressed as

$$-c\nabla x_i = \sum_{j=1, i\neq j}^{n} \frac{1}{D_{ij}} (x_j \vec{N}_i - x_i \vec{N}_j) + \frac{\vec{N}_i}{D_{Kn,i}} \tag{7}$$

where $D_{Kn,i}$ is the Knudsen diffusion coefficient of species i.

Combining the two terms on the right-hand side of Eq. (7), the modified Stefan–Maxwell equations are expressed as

$$-c\nabla x_i = \sum_{j=1, i\neq j}^{n} \frac{1}{\wp_{ij}} (x_j N_i - x_i N_j) \tag{8}$$

where $\wp_{ij}$ is the diffusion coefficient, expressed as

$$\wp_{ij} = \left(\frac{D_{ij} D_{Kn,i}}{D_{ij} + D_{Kn,i}}\right) \tag{9}$$

The effective diffusion coefficient can be obtained using the following relation:

$$\wp_{ij}^{eff} = \frac{\varepsilon}{\tau} \wp_{ij} \tag{10}$$

Replacing the diffusion coefficient with the effective diffusion coefficient, the modified Stefan–Maxwell equation, Eq. (8), becomes

$$-c\nabla x_i = \sum_{j=1, i\neq j}^{n} \frac{1}{\wp_{ij}^{eff}} (x_j N_i - x_i N_j) \tag{11}$$

The species source term on the right-hand side of Eq. (1), represents the rate of production or consumption of species due to the water–gas shift reaction given as

$$CO + H_2O \Rightarrow H_2 + CO_2 \tag{12}$$

The volumetric reaction rate for the shift reaction can be written as

$$r_s = k_{fs} c_{CO} c_{H_2O} - k_{bs} c_{CO_2} c_{H_2} \tag{13}$$

where k_{fs} and k_{bs} are forward and backward reaction rate constants for the water–gas shift reaction.

In terms of mole fraction, the volumetric reaction rate for shift reaction becomes

$$r_s = \left(\frac{p}{RT}\right)^2 [k_{fs} x_{CO} x_{H_2O} - k_{bs} x_{CO_2} x_{H_2}] \tag{14}$$

where p is the total pressure, R is the universal gas constant and T is the temperature.

The mass rates of production or consumption of various species due to water–gas shift reaction in the anode electrode and reaction zone layers can be formulated as follows:

$$\dot{S}_{s,H_2} = M_{H_2} r_s \tag{15}$$

$$\dot{S}_{s,H_2O} = -M_{H_2O} r_s \tag{16}$$

$$\dot{S}_{s,CO} = -M_{CO} r_s \tag{17}$$

$$\dot{S}_{s,CO_2} = M_{CO_2} r_s \tag{18}$$

where M_{H_2}, M_{H_2O}, M_{CO}, and M_{CO_2} are the molecular weights of H_2, H_2O, CO and CO_2, respectively.

The species source term in the anode reaction zone layer due to electrochemical oxidation of H_2 is related to volumetric current density produced through the Faraday's law of electrochemical reaction and is described as follows

$$\dot{S}_{s,i} = -\frac{\nu_i M_i \Re_a}{nF} \tag{19}$$

where M_i is the molecular weight of the species i, $\Re_a$ is the volumetric current density produced in the anode reaction zone layer given in Eq. (5), n is the number of electrons participating in the electrochemical reaction, F is the Faraday's constant, and ν_i is the stoichiometric coefficient of the species expressed in the following form [14]:

$$H_2 + O^{2-} - H_2O \rightarrow 2e^- \tag{20}$$

Expressing the electronic and ionic current densities given in Eqs. (2)–(4) as gradients of electronic and ionic potentials through Ohm's law, Eqs. (2)–(4) becomes

Electronic Charge – Electrode Layer:

$$\nabla \cdot (\sigma_{bl}^{eff} \nabla \phi_e) = 0 \tag{21}$$

Electronic charge – reaction zone layer:

$$\nabla \cdot \left(\sigma_{rl}^{eff} \nabla \phi_e\right) = -\Re_a \tag{22}$$

Ionic charge – reaction zone layer:

$$\nabla \cdot \left(\kappa_{rl}^{eff} \nabla \phi_i\right) = \Re_a \tag{23}$$

where the effective electronic conductivity in the electrode layer and effective electronic and ionic conductivities in the reaction zone layer are defined as [15]:

$$\sigma_{bl}^{eff} = \left(\frac{1-\varepsilon}{\tau}\right)\sigma \tag{24}$$

$$\sigma_{rl}^{eff} = \Phi\left(\frac{1-\varepsilon}{\tau}\right)\sigma \tag{25}$$

$$\kappa_{rl}^{eff} = (1-\Phi)\left(\frac{1-\varepsilon}{\tau}\right)\kappa \tag{26}$$

where Φ is the volume fraction of the electron conducting particles in the reaction zone layer, σ and κ are the conductivities of pure electron and ion-conducting materials, respectively.

As the electric current is drawn from the cell, the reactant concentration at the reaction sites is lower than the concentration in the bulk reactant region. The difference in reactant concentration at the reaction sites and the bulk reactant region leads to a loss in cell potential referred to as the concentration overpotential. In terms of mole fractions, it can be expressed as

$$\eta_{con} = \frac{RT}{nF} \ln\left[\frac{x_{H_2}^a x_{H_2O}^b}{x_{H_2}^b x_{H_2O}^a}\right] \tag{27}$$

where n is the moles of electron produced per mole of reactant consumed, F is the Faraday's constant (96 487 C mole^{-1}), and $x_{H_2}^a$, $x_{H_2}^b$, $x_{H_2O}^a$, and $x_{H_2O}^b$ are the mole fractions of H_2 and H_2O at locations 'a' and 'b', respectively, as shown in Fig. 1.

The locations at which boundary conditions are required to solve the above governing equations are labeled as 'a', 'b' and 'c' in Fig. 1. The interface between the fuel channel and the electrode (backing) layer designated as 'a' in Fig. 1, is a specified (Dirichlet) boundary condition where the composition of species and electronic potential are specified. At location 'b', the interface between the electrode (backing) and reaction zone layers, the diffusive flux of species and electronic current density are continuous; whereas ionic current density is zero. At location 'c', mass flux and electronic current density are zero; whereas ionic current density is equal to the total current density. Mathematically, the boundary conditions can be written as

- At $x =$ 'a': $x_i =$ specified $\quad \phi_e =$ specified
- At $x =$ 'b': $N_i|_{bl} = N_i|_{rl}$, $\quad J_e|_{bl} = J_e|_{rl}$, $\quad J_i = 0$
- At $x =$ 'c': $N_i = 0$, $\quad J_e = 0$, $\quad J_i = J$

3. Numerical implementation

The mathematical model presented above is based on the conservation principle. Therefore, the numerical method used to discretize the governing equations is a well-known method, referred to as 'finite-volume method'. The discretized governing equations form a system of algebraic equations whose solution can be obtained using a direct method or an iterative method. For the problem at hand, an iterative method is used because of the fact that the coefficients of the discretized algebraic equations are functions of the variables evaluated at grid points.

4. Results and discussion

The fuel composition and the base-case parameters used in the simulation are listed in Tables 1 and 2, respectively. Since

Table 1
Mole fractions of ethanol reformate fuel used in the simulation

Mole fraction	Value
x_{H_2}	0.480
x_{H_2O}	0.200
x_{CO}	0.220
x_{CO_2}	0.100

Source: Breen et al. [16].

Table 2
Base-case parameters used in the simulation

Parameter	Value
Operating temperature, T_{op}	1073.0 K
Total pressure, p	1.0 atm
Electrode layer thickness, t_a	2000.0 μm [7]
Reaction zone layer thickness, t_{arz}	50.0 μm [7]
Porosity, ε	0.3 [17]
Tortuosity, τ	4.5 [6]
Pore diameter, d_p	1.0 μm [17]
Volume fraction of electron conducting particles in the reaction zone, Φ	0.5 [18]
Reactive area per unit volume, A_v	0.5×10^6 m^2 m^{-3} [18]
Reference current density, $J_{0,ref}^{H_2}$	1320 A m^{-2} [5]
Reaction order, γ_{H_2}	0.5
Electronic conductivity, σ	$\frac{9.5\times10^7}{T}\exp(-\frac{1150}{T})$ S m^{-1} [19]
Ionic conductivity, κ	$3.34 \times 10^4 \exp(-\frac{10300}{T})$ S m^{-1} [19]

the model is fuel flexible which can predict the distribution of various species in the porous electrode and reaction zone layers for any reformate composition, ethanol reformate fuel composition obtained from Breen et al. [16] is used in the present simulation. Water–gas shift reaction is also considered in the electrode and reaction zone layers involving production of additional H_2 for electrochemical reaction at the reaction sites.

Fig. 2 shows the distribution of species mole fraction in the electrode and reaction zone layers at 0.7 A cm^{-2}. The abscissa of Fig. 2(a) and (b) represents the non-dimensionalized electrode and reaction zone thickness, respectively; whereas the ordinate of Fig. 2(a) and (b) represents species mole fraction. The temperature and pressure were set at 1073.0 K and 1.0 atm. Since SOFC is typically operated in the range 0.5–0.7 A cm^{-2}, the species distribution is predicted at 0.7 A cm^{-2}. It can be seen that, the concentration or mole fraction of H_2 decreases in the electrode and reaction zone layers as we from the fuel channel side to the electrolyte side, whereas the concentration or mole fraction of H_2O increases from left to right. This is due to the electrochemical oxidation of H_2 at the reaction sites in the reaction zone layer, resulting in production of electrons with H_2O. Although the profiles of species mole fraction seems to be linear but they are varying in a non-linear fashion as we move from fuel channel side to the electrolyte side. This can be evident from Figs. 3 and 4, which depicts the mole fraction distribution of H_2 and H_2O in the electrode and reaction zone layers at different current densities (loads), respectively. This non-linear variation of species in the electrode layer is due to water–gas shift reaction; whereas it is due to water–gas shift reaction and electrochemical oxidation reaction in the reaction zone layer. Further, it can be seen from Figs. 3 and 4 that, with the increase of current density, the mole fraction of H_2 decreases and the mole fraction of H_2O increases. This is attributed to the increase in consumption of H_2 and production of H_2O at the reaction sites in the reaction zone layer in order to meet the desired load.

The effect of shift reaction on the concentration overpotential is shown in Fig. 5. The operating and design parameters are same as the base-case parameters listed in Table 2. The x-axis represents the current density or load, whereas y-axis represents the concentration overpotential. It can be observed that concentration overpotential increases with the increase of current density. This is due to decrease in reactant concentration at the reaction sites. With the increase of current density, the rate of electrochemical H_2 oxidation at the reaction sites increases in order to meet the desired output requirement. As a result, the reactants are consumed rapidly at the reaction sites. The lim-

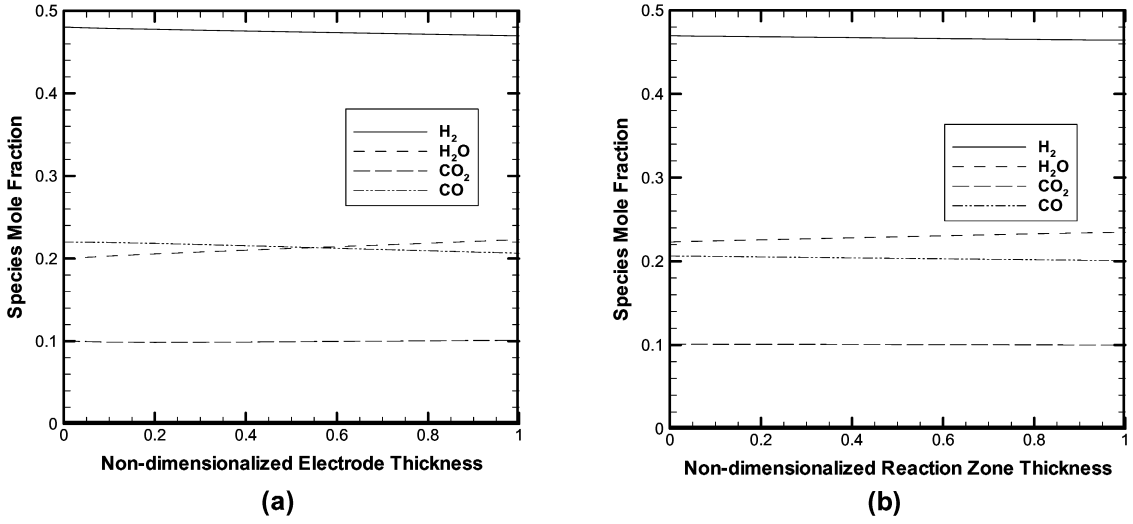

Fig. 2. Distribution of species mole fraction in the electrode and reaction zone layers at 0.7 A cm^{-2}.

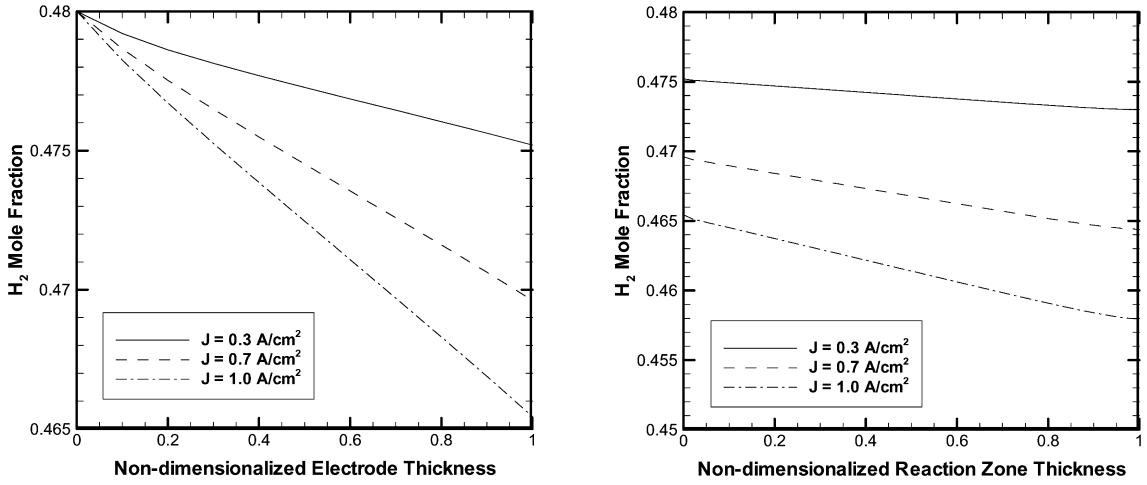

Fig. 3. Distribution of H_2 mole fraction in the electrode and reaction zone layers at different current densities.

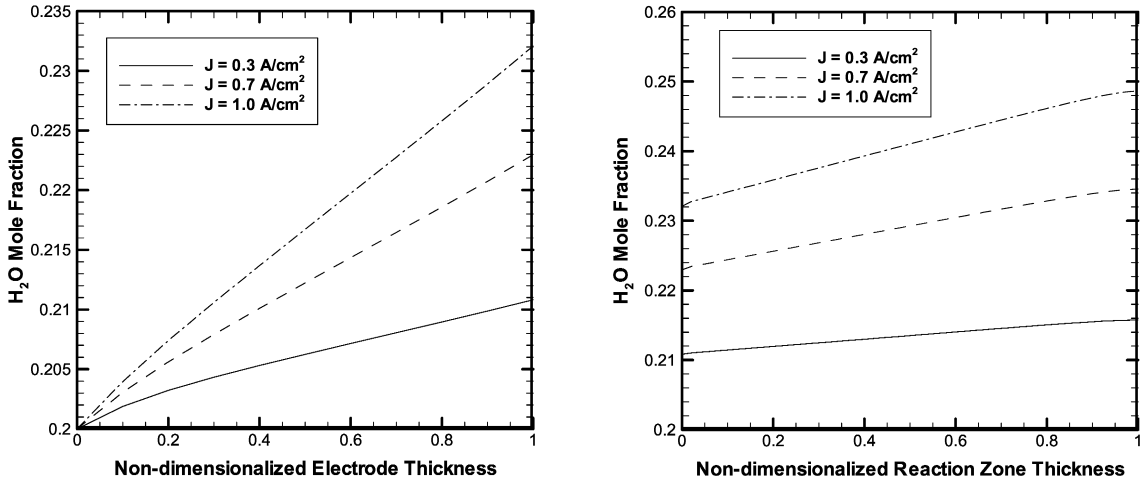

Fig. 4. Distribution of H_2O mole fraction in the electrode and reaction zone layers at different current densities.

ited rate of mass transfer results in lower reactant concentration at the reaction sites leading to increased concentration overpotential at higher loads. It can also be seen that, the water–gas shift reaction in the anode results in decreasing the concentration overpotential at higher current densities. This is due to production of additional H_2 during shift reaction resulting in higher reactant concentration at the reaction sites. Further, it can be observed that the decrease in concentration overpotential through water–gas shift reaction is insignificant with the present ethanol fuel reformate composition, as the rate of water–gas shift reaction depends on the concentration of CO and H_2O and temperature.

Fig. 6 shows the effect of considering finite reaction zone layer on concentration overpotential. Again the operating and design conditions are same as the base-case parameters listed in Table 2. From the figure, it can be seen that the consideration of reaction zone layer as a mathematical surface result in overpredicting the concentration overpotential at all loads considered in the simulation. This is due to sudden drop in concentration of the reactants at the reactant sites in the case of no reaction zone layer as compared to the case with reaction zone layer,

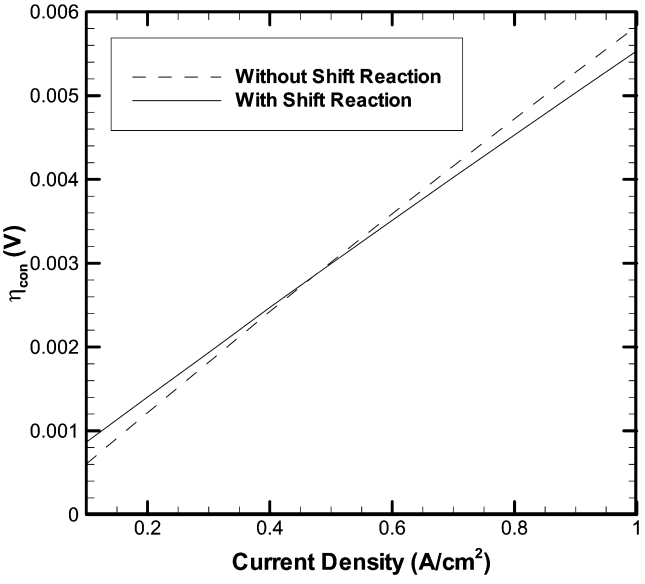

Fig. 5. Effect of shift reaction on the concentration overpotential.

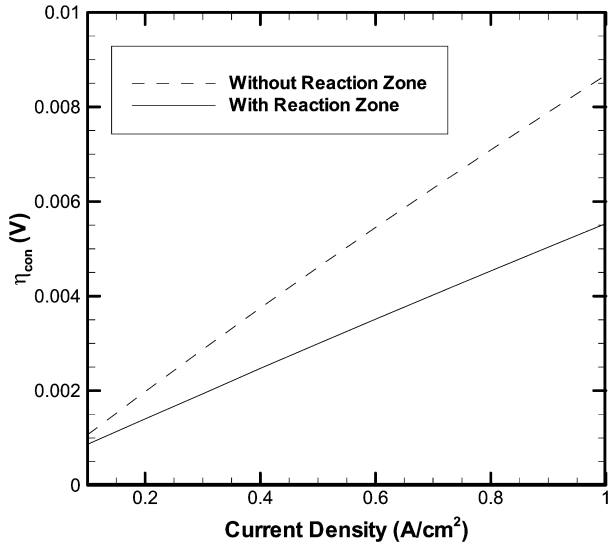

Fig. 6. Effect of reaction zone on concentration overpotential.

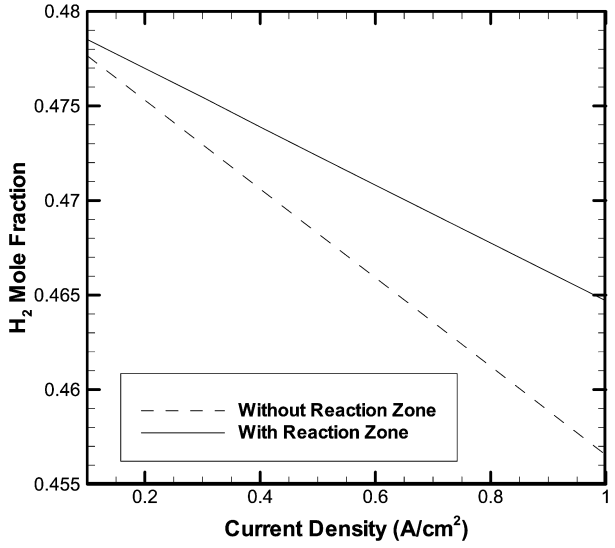

Fig. 7. Mole fraction of H_2 at the interface between the electrode and reaction zone layers.

which is evident from Fig. 7. The sudden decrease in reactant concentration in case of no reaction zone layer is due to single reaction site or triple phase boundary (TPB) as compared to multiple reaction sites or triple phase boundaries (TPBs) spread over the finite reaction zone layer (Williford and Chick, 2003). Moreover, it can be observed that the magnitude of concentration overpotential is less significant at all the loads considered in the present simulation. Therefore, other overpotentials such as activation and ohmic has to be predicted in order to obtain the true performance of the anode under various operating and design conditions.

Fig. 8 shows the distribution of non-dimensionalized electronic potential in the electrode layer at different current densities. The operating and design parameters were set as base-case parameters listed in Table 2. Since there is no electrochemical reaction in the anode electrode layer, the distribution of

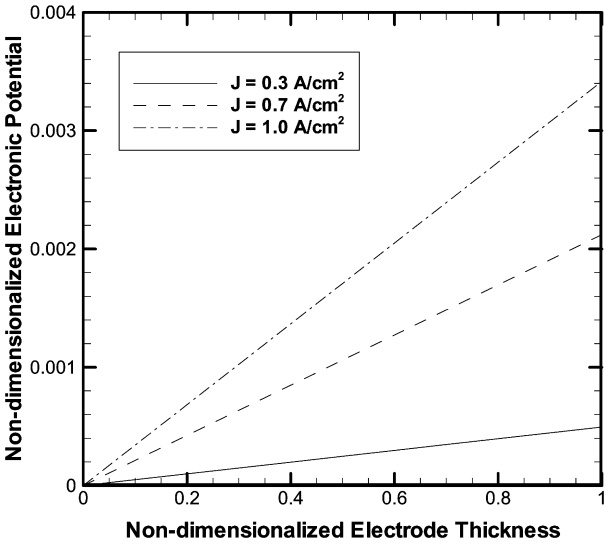

Fig. 8. Non-dimensionalized electronic potential in the electrode layer at different current densities.

non-dimensionalized electronic potential is linear and increases from the left to the right, i.e., from the fuel channel to the reaction zone layer. It can also be seen that the non-dimensionalized electronic potential increases with the increase of current density. This is due to the increased consumption of reactants in the reaction zone layer resulting in the higher electronic potential in order to meet the desired load.

The distribution of non-dimensionalized electronic and ionic potentials in the reaction zone layer at different current densities is shown in Fig. 9. From the figure, it can be seen that the electronic potential increases and the ionic potential decreases from the left to the right, i.e., from anode electrode layer to electrolyte layer. This is due to the transfer of charge from the electrolyte phase to electrode phase in the reaction zone layer. Moreover, it can be seen that, both the electronic and ionic potentials increases with the increase of current density.

The non-dimensionalized electronic and ionic current densities in the reaction zone layer are shown in Fig. 10. The operating and design parameters were set as base-case parameters listed in Table 2. It can be seen that electronic current density increases and ionic current density decreases from the electrolyte layer to the anode electrode layer. This is again due to the transfer of charge from ion-conducting phase to the electron-conducting phase of the anode reaction zone layer.

5. Conclusions

A mathematical model describing the transport of multi-component species inside the porous SOFC anodes has been developed. The model considers reaction zone layer as a finite volume rather than a mathematical surface as treated in the existing models and includes the water–gas shift reaction in the electrode and reaction zone layers. The modified Stefan–Maxwell equations incorporating Knudsen diffusion are used to model the multi-component diffusion inside the porous anode. The general Butler–Volmer equation is used to model the rate of

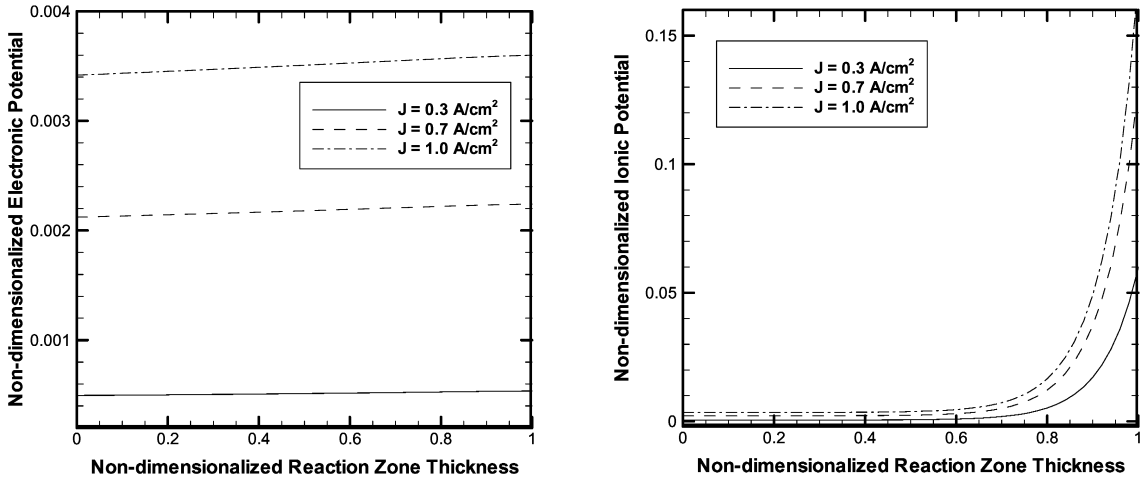

Fig. 9. Non-dimensionalized electronic and ionic potentials in the reaction zone layer at different current densities.

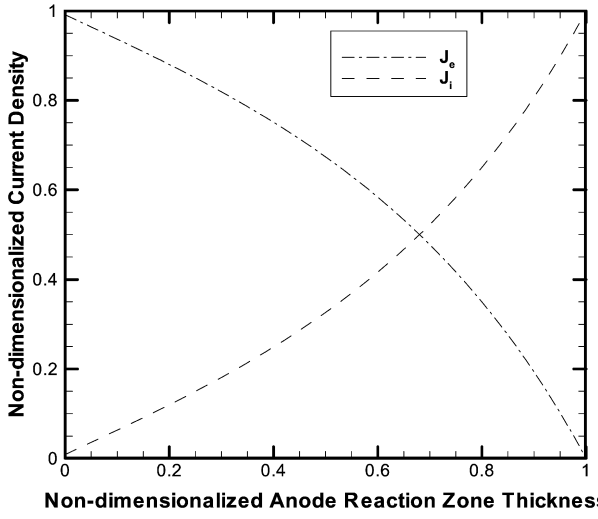

Fig. 10. Non-dimensionalized current densities in the reaction zone layer.

electrochemical reaction in the reaction zone layer. Simulations are then performed using multi-component ethanol reformate fuel to predict the distribution of multi-component species in the electrode and reaction zone layers at different loads (current densities). In addition, the effect of shift reaction and finite reaction zone layer on the concentration overpotential is examined. It is found that, the water–gas shift reaction in the anode results in decreasing the concentration overpotential at higher current densities. Further, it is observed that the decrease in concentration overpotential through water–gas shift reaction is insignificant with the present ethanol fuel reformate composition. It is also found that the consideration of reaction zone layer as a mathematical surface result in overpredicting the concentration overpotential at all loads considered in the simulation. In addition, it is observed that the magnitude of concentration overpotential is less significant at all the loads considered in the present simulation. Therefore, other overpotentials such as activation and ohmic has to be predicted in order to obtain the true performance of the anode under various operating and design conditions.

References

[1] R.J. Gorte, Recent developments towards commercialization of solid oxide fuel cells, AIChE Journal 51 (2005) 2377–2381.

[2] K.P. Recknagle, R.E. Williford, L.A. Chick, D.R. Rector, M.A. Khaleel, Three-dimensional thermo-fluid electrochemical modeling of planar SOFC stacks, Journal of Power Sources 113 (2003) 109–114.

[3] M.A. Khaleel, Z. Lin, P. Singh, W. Surdoval, D. Collin, A finite element analysis modeling tool for solid oxide fuel cell development: coupled electrochemistry, thermal and flow analysis in MARC, Journal of Power Sources 130 (2004) 136–148.

[4] R. Maric, S. Ohara, T. Fukui, H. Yoshida, M. Nishimura, T. Inagaki, K. Miura, Solid oxide fuel cells with doped lanthanum gallate electrolyte and $LaSrCoO_3$ cathode, and Ni-samaria-doped ceria cermet anode, Journal of the Electrochemical Society 146 (1999) 2006–2010.

[5] J.W. Kim, A.V. Virkar, K.-Z. Fung, K. Mehta, S.C. Singhal, Polarization effects in intermediate temperature, anode-supported solid oxide fuel cells, Journal of the Electrochemical Society 146 (1999) 69–78.

[6] H. Yakabe, M. Hishinuma, M. Uratani, Y. Matsuzaki, I. Yasuda, Evaluation and modeling of performance of anode-supported solid oxide fuel cell, Journal of Power Sources 86 (2000) 423–431.

[7] W. Lehnert, J. Meusinger, F. Thom, Modelling of gas transport phenomena in SOFC anodes, Journal of Power Sources 87 (2000) 57–63.

[8] R. Suwanwarangkul, E. Croiset, M.W. Fowler, P.L. Douglas, E. Entchev, M.A. Douglas, Performance comparison of Fick's, dusty–gas and Stefan–Maxwell models to predict the concentration overpotential of a SOFC anode, Journal of Power Sources 122 (2003) 9–18.

[9] C.W. Tanner, K.Z. Fung, A.V. Virkar, Effect of porous composite electrode structure on solid oxide fuel cell performance. I. Theoretical analysis, Journal of the Electrochemical Society 144 (1997) 21–30.

[10] A. Bieberle, L.P. Meier, L.J. Gauckler, The electrochemistry of Ni pattern anodes used as solid oxide fuel cell model electrodes, Journal of the Electrochemical Society 148 (2001) A646–A656.

[11] X.J. Chen, S.H. Chan, K.A. Khor, Simulation of a composite cathode in solid oxide fuel cells, Electrochimica Acta 49 (2004) 1851–1861.

[12] R. Taylor, R. Krishna, Multicomponent Mass Transfer, Wiley Series in Chemical Engineering, Wiley, New York, 1993.

[13] S.H. Chan, K.A. Khor, Z.T. Xia, A complete polarization model of a solid oxide fuel cell and its sensitivity to the change of cell component thickness, Journal of Power Sources 93 (2001) 130–140.

[14] J. Newman, K.E. Thomas-Alyea, Electrochemical Systems, third ed., Wiley, New Jersey, 2004.

[15] J. Deseure, Y. Bultel, L. Dessemond, E. Siebert, Theoretical optimization of a SOFC composite cathode, Electrochimica Acta 50 (2005) 2037–2046.

[16] J.P. Breen, R. Burch, H.M. Coleman, Metal-catalysed steam reforming of ethanol in the production of hydrogen for fuel cell applications, Applied Catalysis B: Environmental 39 (2002) 65–74.
[17] S. Sunde, Simulations of composite electrodes in fuel cells, Journal of Electroceramics 5 (2000) 153–182.
[18] P. Costamagna, P. Costa, V. Antonucci, Micro-modelling of solid oxide fuel cell electrodes, Electrochimica Acta 43 (1998) 375–394.
[19] J.R. Ferguson, J.M. Fiard, R. Herbin, Three-dimensional numerical simulation for various geometries of solid oxide fuel cells, Journal of Power Sources 58 (1996) 109–122.